



Photocatalytic activity of nano-ZnO loaded with Ag and Fe immobilized on ZSM-5

Hang Xu*, Dandan Zhang, Fengmin Wu

Chemical Engineering and Pharmaceutics School, Henan University of Science and Technology, Luoyang 471023, China, Tel. +86-379-64231914; emails: xhinbj@126.com (H. Xu), 394720738@qq.com (D. Zhang), min49@126.com (F. Wu)

Received 29 March 2016; Accepted 22 February 2017

ABSTRACT

Photocatalysts zinc oxide (ZnO)/ZSM-5, Fe-ZnO/ZSM-5, Ag-ZnO/ZSM-5, and Ag-Fe-ZnO/ZSM-5 were successfully prepared using sol-gel method. The synthesized photocatalysts were characterized by X-ray diffraction, Brunauer-Emmett-Teller, scanning electron microscopy, transmission electron microscopy, energy-dispersive X-ray spectroscopy, and diffuse reflectance spectroscopy measurements. Photocatalytic activities of the photocatalysts were evaluated by the removal of Rhodamine B and Reactive Red 6B from aqueous solutions under ultraviolet (UV) or visible irradiation. The results show that the size of nano-ZnO on ZSM-5 surface was ~10 nm. Fe and Ag co-loaded nano-ZnO/ZSM-5 effectively suppressed the recombination of photogenerated holes and electrons and reduced the band-gap energy. The photocatalytic process followed first-order kinetics with $>0.98 R^2$. The best Fe- and Ag-loaded amounts were 0.6% and 1%, respectively, exhibiting 80% Rhodamine B removal at 320 min and 100% Reactive Red 6B removal at 280 min under UV irradiation. Ag-Fe-ZnO/ZSM-5 expressed an outstanding photocatalytic performance under visible-light irradiation with 67% Rhodamine B removal at 320 and 0.0034 min^{-1} reaction rate constant. Ag-Fe-ZnO/ZSM-5 was used three times without any inactivation.

Keywords: Ag loaded; Fe loaded; Nano-ZnO/ZSM-5; Photocatalytic activity; Rhodamine B

1. Introduction

Zinc oxide (ZnO) exhibits excellent characteristics in many fields such as ceramics, catalysis, electronics, biology, and medicine [1–5]. The preparation and application of ZnO have been extensively studied. Nano-ZnO is a superior photocatalyst because when the wavelength of incident light is smaller than 380 nm [6], the electrons in the valence band of ZnO will be excited to the conduction band, and photogenerated holes will be produced in the valence band. Next, the photogenerated holes react with adsorbed H_2O on the surface of ZnO, producing hydroxyl radicals ($\cdot\text{OH}$) that possess outstanding oxidative ability for the degradation of organic contaminants [7].

However, the application of nano-ZnO in the photocatalytic field suffers from some problems. First, nanoparticles

suffer from the recovery difficulty, severely hindering their application in actual wastewater treatment. On the other hand, the band-gap energy (3.37 eV) of ZnO is so high that more energy should be provided to excite electrons from the conduction band to the valence band, i.e., the incident light should be in the ultraviolet (UV) zone ($<380 \text{ nm}$). To overcome the deficiencies, nano-ZnO should be modified. Nano-ZnO particles can be immobilized on a special carrier, solving the problem of catalyst recycle. In previous study, we prepared nano-ZnO supported on bentonite that exhibited a great photocatalytic activity for Acid Yellow 11 degradation [8]. Xu et al. [9] prepared nano-ZnO/sepiolite to solve the problem of catalyst recovery. Metal-loaded ZnO can also improve the photocatalytic activity. Choi et al. [10] prepared Ag/ZnO to improve light utilization, thus increasing the photocatalytic activity. Yi et al. [6] selected Fe-loaded ZnO to enhance visible-light photocatalytic activity for the degradation of

* Corresponding author.

Rhodamine B. Saleh and Djaja [11] also prepared Fe-loaded ZnO nanoparticles for the UV-light photocatalytic degradation of organic dyes in aqueous media.

ZSM-5 is a molecular sieve with a regular periodic structure, a large surface area, strong adsorption, and high chemical stability. It can be widely used as a carrier, especially in the photocatalytic field. Khatamian et al. [12] used hydrothermal method to prepare metal-ion-loaded TiO₂ nanoparticles supported on ZSM-5 zeolite, and Fe-TiO₂/ZSM-5 catalyst showed the best photocatalytic activity. Zhang et al. [13] selected HZSM-5 as the carrier to immobilize SrTiO₃, and a high adsorption of HZSM-5 was the advantage for a high photocatalytic performance. TiO₂-loaded ZSM-5 has been extensively studied. However, nano-ZnO-loaded ZSM-5 has been rarely studied.

In this study, nano-ZnO-loaded ZSM-5 was prepared for the degradation of organic dyes, non-azo dye Rhodamine B, and azo dye Reactive Red 6B, in aqueous media under UV-light or visible-light irradiation. Metal ions, Ag and Fe, were loaded in nano-ZnO using the sol-gel method. The photocatalysts were characterized by X-ray diffraction (XRD), scanning electron microscopy (SEM), transmission electron microscopy (TEM), energy-dispersive X-ray spectroscopy (EDX), Brunauer-Emmett-Teller (BET), and diffuse reflectance spectroscopy (DRS).

2. Experimental

2.1. Synthesis of materials

First, 1.1 g zinc acetate, 0.0072 g Fe(NO₃)₃ and/or 0.0085 g AgNO₃ were dissolved in 50 mL anhydrous ethanol at 80°C. Then, 0.405 g ZSM-5 (Si:Al = 25) was added to the zinc acetate solution, forming a hybrid system. A solution of 0.29 g lithium hydroxide in 50 mL anhydrous ethanol and 100 mL of *n*-hexane were added to the hybrid system at room temperature. A white gel was obtained after standing overnight at 4°C. The precursor was obtained by centrifugation and drying at 100°C. The Ag-Fe-ZnO/ZSM-5 composite powder was prepared by calcination at 200°C for 4 h [8].

2.2. Characterization of materials

The crystal phase of the sample was analyzed by XRD using a PANalytical X-ray diffractometer (X'Pert Pro MPD, Netherlands) using Cu K α radiation. SEM was performed using a Nova NanoSEM (FEI, USA) equipped with EDX. TEM was carried out using a JEM-2010 (JEOL, Japan). UV-visible DRS of the samples was obtained using an AvaSpec-2048 TEC spectrometer for the determination of the optical band gap (E_g) of impregnated catalysts. The specific surface area was calculated using the BET method using the Quantachrome Autosorb 1 software (USA).

2.3. Photocatalytic activity tests

Rhodamine B, a non-azo dye, was used to investigate the photocatalytic performance. The maximum absorption wavelength of Rhodamine B was 553 nm. To evaluate the photocatalytic activity, 200 mL of 20 mg/L Rhodamine B and 0.1 g/L photocatalyst were added to a 250 mL beaker under magnetic

stirring. A 10-cm-long mercury UV lamp (10 W Guangdong Bright Star) was used as the radiation source with a wavelength of 245 nm. The visible-light irradiation experiment was carried out using a 300-W halogen lamp (Osram, Germany) equipped with a cutoff filter, which completely filtered the light of wavelengths shorter than 400 nm and ensured that the photocatalytic system was irradiated by visible light only. The light site was above the reaction liquid. After a certain reaction interval of 40 min, a 10-mL sample was removed and centrifuged at 12,000 rpm to remove the catalyst. The dyestuff absorbance of Rhodamine B was analyzed using a UV-2102PC UV-visible spectrophotometer (UNICO, China). The degradation rate of Rhodamine B was calculated using Eq. (1):

$$\text{Removal \%} = [(C_0 - C_t)/C_0] \times 100\% \quad (1)$$

where C_0 is the initial concentration of Rhodamine B, and C_t is the concentration of Rhodamine B at time t .

In this study, an azo dye, Reactive Red 6B, was also selected to evaluate the photocatalyst activity. The maximum absorption of Reactive Red 6B was 523 nm. The photocatalytic experiment was carried out in the same manner as the Rhodamine B degradation.

3. Results and discussion

3.1. XRD and BET analyses

Fig. 1 clearly shows that most of the diffraction peaks of ZSM-5 are $<30^\circ$, very similar to that reported in the literature [13–15]. The three main peaks are located at 2θ values of 23° , 23.8° , and 24.2° in the XRD patterns of Ag-Fe-ZnO/ZSM-5 and ZnO/ZSM-5. Fig. 1 shows the diffraction peaks of ZnO at 2θ values of 31.7° , 34.4° , 36.2° , 47.5° , 56.5° , 62.8° , 67.9° , and 68.8° . All the peaks can be well indexed to standard patterns (JCPDS 36-1451) without any impurity phase. The major peaks of ZnO at 2θ values of 31.7° , 34.4° , 36.2° , and 47.5° can be attributed to (100), (002), (101), and (102) crystal planes, respectively [16,17]. In the XRD pattern of Ag-Fe-nano-ZnO/ZSM-5, the diffraction peaks at 35.7° , 43.4° , and 64.8° can be attributed to the Ag phase (JCPDS 04-0783) [16]. A low amount of Ag leads to the low intensity of diffraction

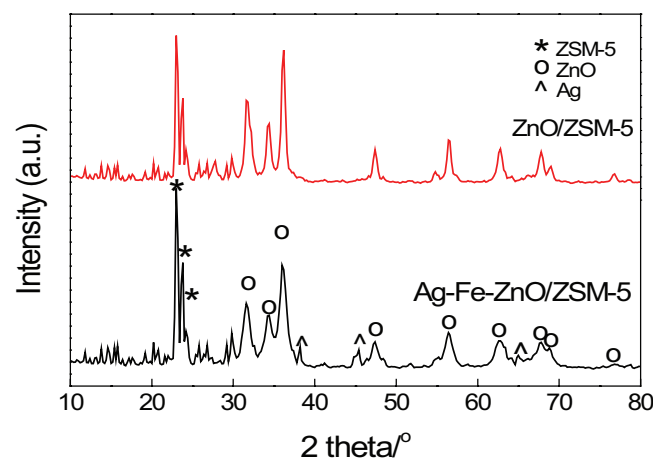


Fig. 1. XRD of Ag-Fe-nano-ZnO/ZSM-5 and nano-ZnO/ZSM-5.

peaks in the XRD pattern. The amount of Fe is so low that no diffraction peak was observed in the XRD pattern of Ag-Fe-nano-ZnO/ZSM-5. The intensity of the diffraction peaks in the XRD patterns of ZnO in Ag-Fe-nano-ZnO/ZSM-5 is slightly higher than that in nano-ZnO/ZSM-5. Metal ion is advantageous for the crystallinity of ZnO in loaded composite materials. The half-peak width in the XRD patterns clearly indicates that the particle size of ZnO in nano-ZnO/ZSM-5 is slightly larger than that in Ag-Fe-nano-ZnO/ZSM-5. Metal loaded in ZnO increased the particle size of ZnO in the composite materials. The average particle sizes of ZnO in Ag-Fe-nano-ZnO/ZSM-5 and nano-ZnO/ZSM-5 were obtained using the Scherrer equation $D = K\lambda/\beta\cos\theta$, where, D is the average crystallite size, λ is the X-ray wavelength, θ is the Bragg angle, β is the corrected half-peak width of the experimental sample, and K is the shape factor with a value of 0.9 [17]. The average crystal sizes of ZnO in ZnO/ZSM-5 and Ag-Fe-ZnO/ZSM-5 were 9.6 and 10.2 nm, respectively.

The BET surface areas of ZSM-5 and Ag-Fe-ZnO/ZSM-5 were 407 and 372 m²/g, respectively, as per the N₂ physisorption experiment. Loaded Ag-Fe-ZnO slightly affected the specific surface area of the carrier ZSM-5.

3.2. SEM, EDX, and TEM analyses

Fig. 2 shows the SEM images (a) and (b), EDX (c), and TEM images (d) and (e) of Ag-Fe-nano-ZnO/ZSM-5. Fig. 2(a) clearly shows that ZSM-5 contains micron-sized solid powders that can be easily separated from water using only simple gravity sedimentation. Fig. 2(b) shows spherical ZnO nanoparticles on the surface of ZSM-5, and the particle size is very uniform. To observe the microstructure more clearly, the TEM of nano-ZnO was investigated. Figs. 2(d) and (e) show spherical ZnO particles. The particle size is about 10 nm, consistent with the XRD result. To detect the presence of Fe and Ag metals, Ag-Fe-nano-ZnO/ZSM-5 photocatalyst was analyzed by EDX. Fig. 2(c) shows eight elements. According to the EDX, the molar ratio of Si (10.12%) and Al (0.39%) is 25.9. In this study, the ingredients in ZSM-5 are Si, Al, and O, and the molar ratio of Si and Al is 25. Ag and Fe were determined, and the contents are 1.1% and 0.58%, respectively. The molar ratio of ZSM-5 and ZnO is 1:1, and 25% Zn content is correct. In theory, C and Cl elements should not be present. The existence of 3.44% C and 1.45% Cl can be attributed to the incomplete washing of the catalyst. The photocatalyst is a composite oxide; therefore, the content of O is up to 51%.

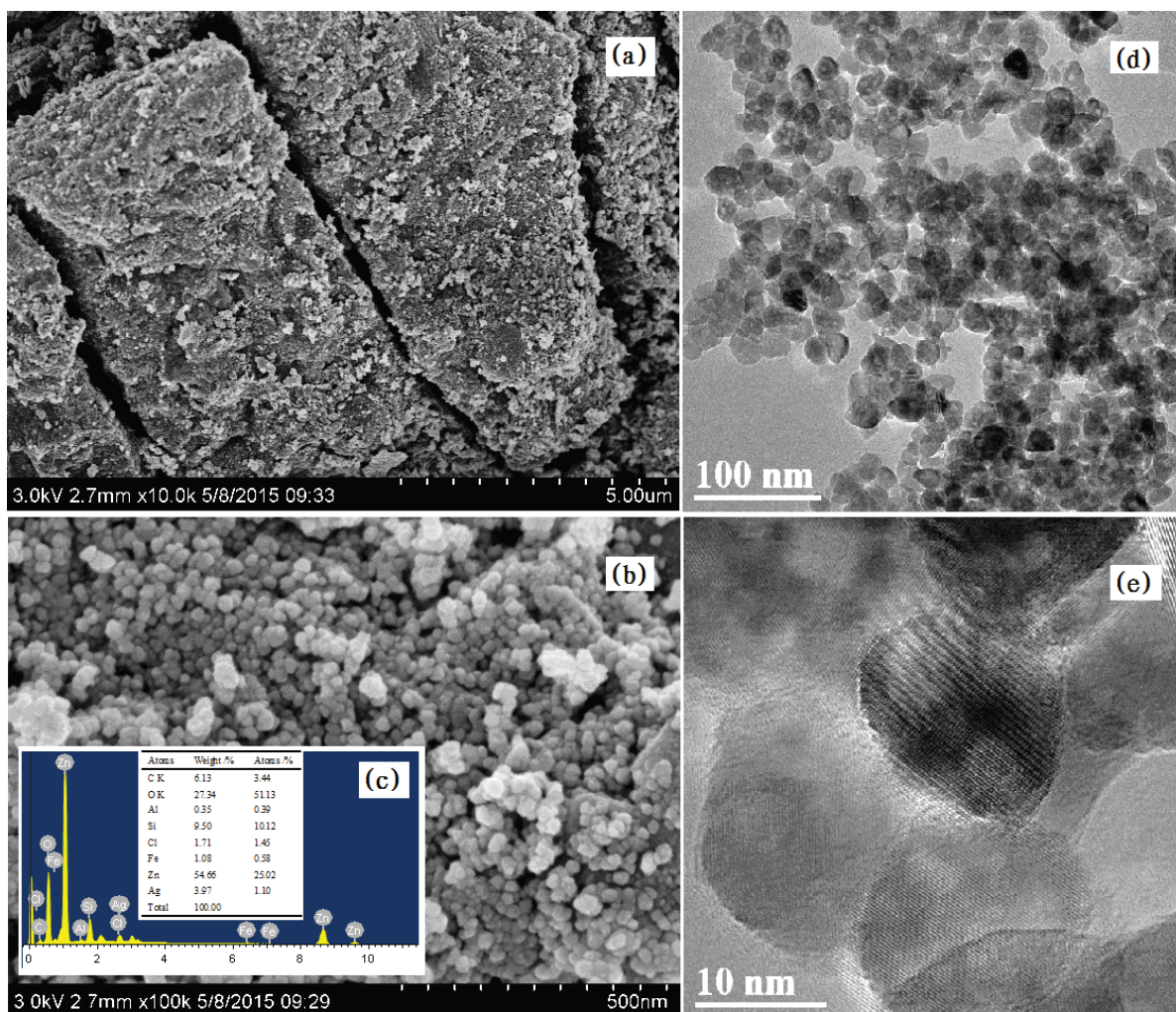


Fig. 2. SEM images ((a) and (b)), EDX (c), and TEM images ((d) and (e)) of Ag-Fe-nano-ZnO/ZSM-5.

3.3. UV-visible DRS

The UV-visible DRS of ZnO/ZSM-5, Fe-ZnO/ZSM-5, Ag-ZnO/ZSM-5, and Ag-Fe-ZnO/ZSM-5 was carried out to investigate the effect of Fe and Ag addition on the optical absorption properties of ZnO. The results are shown in Fig. 3(a). The absorption wavelengths for monometallic-, metallic Fe-, metallic Ag-, bimetallic Fe-, and Ag-loaded ZnO showed a significant redshift phenomenon. The band-gap energies were calculated using the Kubelka-Munk (KM) method [10]. The E_g value was determined using Eq. (2):

$$\alpha(h\nu) = B(h\nu - E_g)^{1/2} \tag{2}$$

where α is the optical absorption coefficient, B is a constant that depends on the transition probability, h is the Planck's constant, and ν is the frequency of the radiation. The E_g value was calculated by plotting $(\alpha h\nu)^2$ vs. $h\nu$, followed by the extrapolation of the linear part of the spectra of the energy axis. The picture of $(\alpha h\nu)^2$ vs. $h\nu$ is shown in Fig. 3(b). Excitation wavelengths (λ) for different photocatalysts were also calculated using Eq. (3):

$$\lambda = E_g / hc \tag{3}$$

where c is the speed of light. The calculated results are shown in Table 1. The band-gap energy (E_g) of pure ZnO/ZSM-5 is ~3.34 eV, and the catalyst can be activated when the wavelength

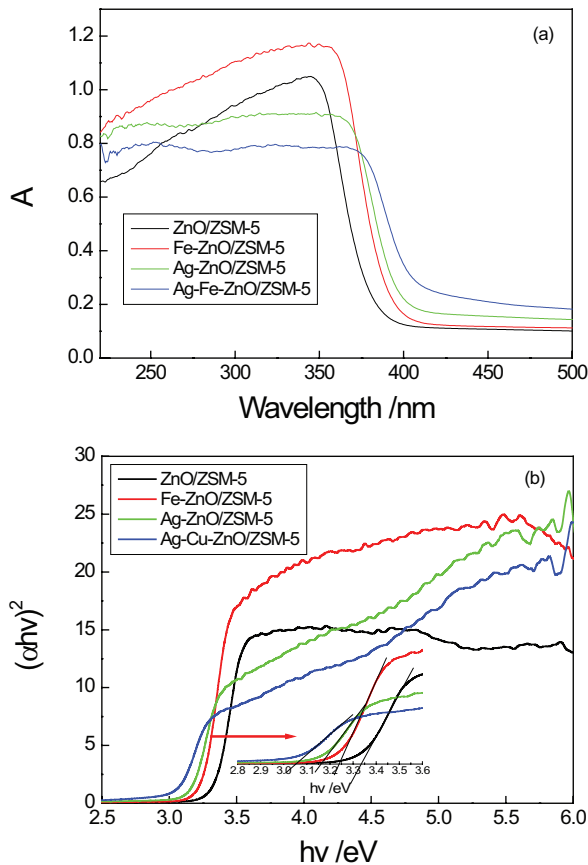


Fig. 3. DRS (a) and plot of $(\alpha h\nu)^2$ vs. $h\nu$ (b) for four photocatalysts.

of incident light should be <371 nm. When 0.6% Fe or 1% Ag was added to ZnO/ZSM-5, the band-gap energy decreased, and the wavelength of incident light increased. The bimetallic Fe- and Ag-loaded ZnO/ZSM-5 had the smallest band-gap energy (3.05 eV), indicating that the wavelength of incident light can be improved to 407 nm (visible zone). Therefore, Fe and Ag can improve the usage efficiency of light, especially visible light.

3.4. Fe impact

Fig. 4 shows the effect of Fe-loaded amount in Fe-nano-ZnO/ZSM-5 photocatalyst on Rhodamine B removal and

Table 1
Band gap and excitation wavelength for four photocatalysts

Photocatalyst	Band-gap energy (eV)	Excitation wavelength (nm)
ZnO/ZSM-5	3.34	371
Fe-ZnO/ZSM-5	3.24	383
Ag-ZnO/ZSM-5	3.16	392
Ag-Fe-ZnO/ZSM-5	3.05	407

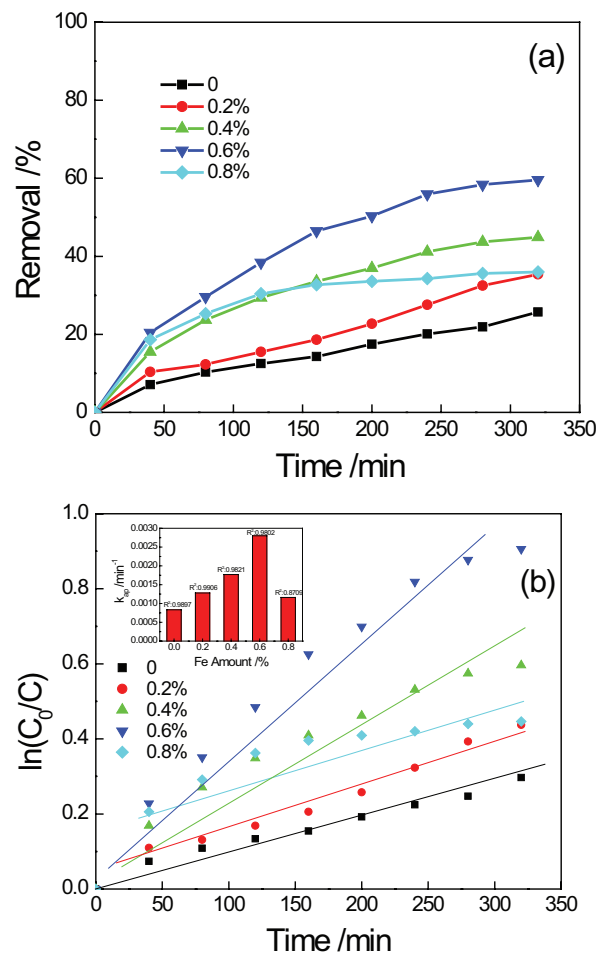


Fig. 4. Rhodamine B removal (a) and first-order kinetics fit (b) at different Fe contents within Fe-nano-ZnO/ZSM-5.

first-order kinetics. Fig. 4(a) clearly shows that Fe amount significantly affected the catalytic performance. Only ~25% Rhodamine B was removed after 320 min without Fe impregnation. When the Fe-loaded amount was increased from 0.2% to 0.6%, the Rhodamine B removal increased from 35.4% to 59.6% after 320 min. The best Fe-loaded amount was 0.6%. After the Fe-loaded amount exceeded 0.6%, the Rhodamine B removal significantly decreased, and only 36% removal was observed after 320 min at 0.8% Fe-loaded amount. According to a large number of reports and our previous research [18–20], the photocatalytic process followed first-order kinetics. The integral form of first-order kinetics is $\ln(C_0/C) = k_{ap}t$, where k_{ap} , t , C_0 , and C are the rate constant, reaction time, and dye concentration at zero time and time t , respectively. Fig. 4(b) shows the results of first-order kinetic fitness based on the experimental data obtained from Fig. 4(a). The k_{ap} values were 0.0008, 0.0013, 0.0018, and 0.0012 min^{-1} at Fe-loaded amounts of 0%, 0.2%, 0.4%, and 0.8%, respectively. The best k_{ap} was 0.0028 min^{-1} at 0.6% Fe loaded. The fitting correlation coefficients were above 0.98 without 0.8% Fe-ZnO/ZSM-5. Fe impregnation significantly increased the ZnO photocatalytic activity. This is because metallic Fe can consume the photogenerated electrons, which can suppress the recombination of photogenerated holes and electrons. The more active holes can react with H_2O molecules adsorbed on the surface of catalyst, producing more hydroxyl radicals than that without Fe impregnation. In contrast, the catalyst activity can be reduced when the Fe-loaded amount exceeds the best dosage. This is because Fe may also act as an electron-hole recombination center, thus decreasing the photocatalytic activity of ZnO [21–23].

3.5. Ag impact

Fig. 5 shows Rhodamine B removal and first-order kinetics at different Ag contents in Ag-nano-ZnO/ZSM-5. Ag impregnation significantly affected the catalytic activity. The best Ag-loaded amount was 1% with 71% Rhodamine B removal at 320 min. When the Ag-loaded amount reached 1.5%, the dye removal decreased to 61.9%. According to the photocatalytic activity results of Ag-nano-ZnO/ZSM-5, Rhodamine B removal using Ag-loaded ZnO is higher than Fe-loaded ZnO by about 11%. A noble-metal-loaded catalyst is usually better than a non-noble-metal-loaded catalyst. Based on the first-order kinetics, the k_{ap} is 0.00389 min^{-1} when 1% Ag-ZnO/ZSM-5 was used. The fitting correlation coefficients are >0.98 without 1.5% Ag-ZnO/ZSM-5, which is only ~0.97. This clearly shows that the dye removal and reaction rate constant of photocatalyst increased with the increase in Ag incorporation and had the best performance at 1% and then decreased with further increase in Ag amount. This is because proper Ag impregnation is advantageous for the separation of electrons and holes, improving the photocatalytic efficiency. Ag impregnation can also increase the rate of electron transfer to dissolved oxygen. Excessive Ag loaded is a disadvantage for catalyst activity. This is because excess Ag can completely occupy the surface of ZnO, resulting in the insufficient utilization of UV light and thus is disadvantageous for the photocatalytic activity. On the other hand, excessive Ag can also provide electron-hole recombination centers that decrease the dye removal.

3.6. Ag-Fe impact under UV and visible-light irradiation

Fig. 6 shows a comparison of Rhodamine B degradation on ZnO/ZSM-5, 0.6% Fe-ZnO/ZSM-5, 1% Ag-ZnO/ZSM-5, and 1% Ag-0.6% Fe-ZnO/ZSM-5 under UV and visible-light irradiation. Fig. 6(a) shows that 1% Ag-0.6% Fe-ZnO/ZSM-5 is the most efficient photocatalyst in the presence of UV irradiation with 80% Rhodamine B removal at 320 min. Fig. 6(b) shows a high degradation efficiency with 67% Rhodamine B removal at 320 min under visible-light excitation condition. However, according to the first-order reaction rate constants observed in Fig. 6(c), the photocatalytic activity under UV irradiation is better than visible light. The k_{ap} values are 0.005 and 0.0034 min^{-1} under UV and visible-light irradiation, respectively, in the presence of 1% Ag-0.6% Fe-ZnO/ZSM-5 catalyst. Under UV-light irradiation, most of the holes and electrons are produced and recombined. Ag and Fe can capture the photogenerated electrons, and preventing hole-electron recombination, which can improve the photocatalytic efficiency. The Ag and Fe co-loaded nano-ZnO can decrease the band-gap energy of nano-semiconductor photocatalyst, and the light absorption wavelength showed a redshift phenomenon. Therefore, Ag-Fe-ZnO/ZSM-5 shows remarkable activity under visible-light irradiation.

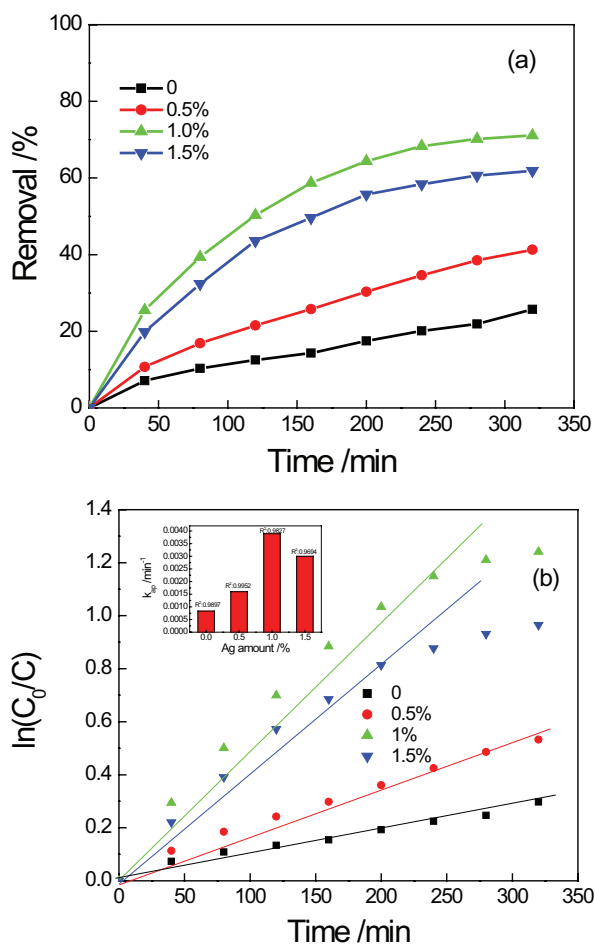


Fig. 5. Rhodamine B removal (a) and first-order kinetics fit (b) at different Ag contents within Ag-nano-ZnO/ZSM-5.

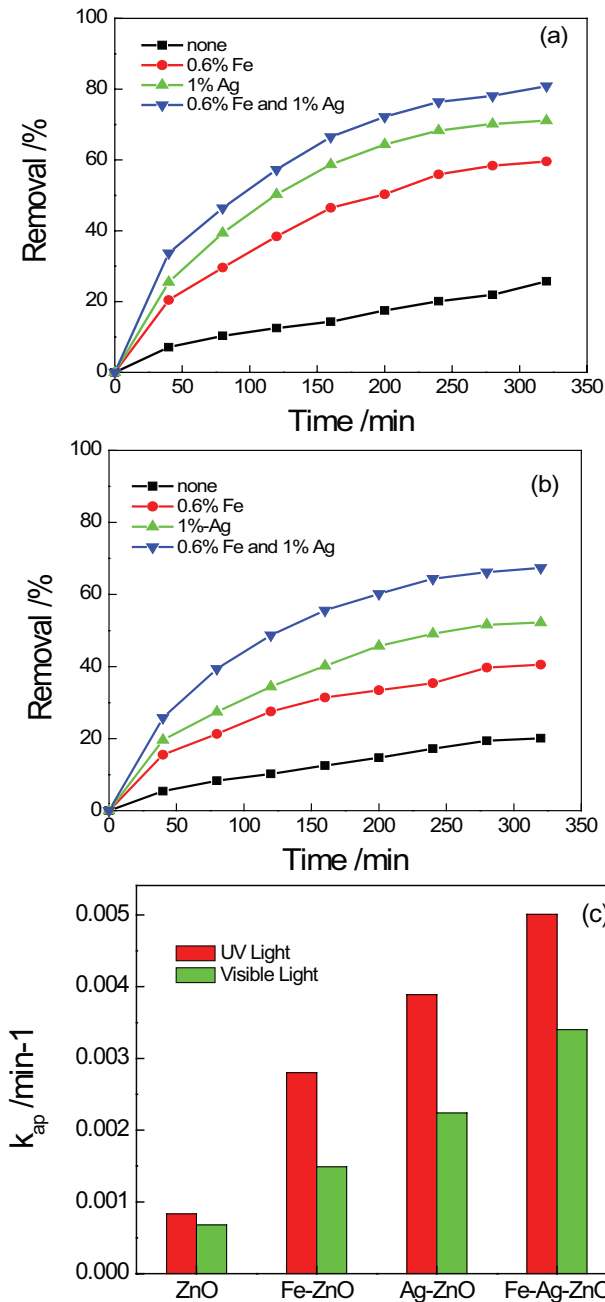


Fig. 6. Rhodamine B degradation under UV (a) and visible light (b) at different catalysts and reaction rate constants (c).

3.7. ZSM-5 impact

Fig. 7 shows the removal of Rhodamine B under UV-light irradiation using only Ag-Fe-ZnO, ZSM-5, and Ag-Fe-ZnO/ZSM-5 as the photocatalysts. Clearly, only 5% Rhodamine B removal was observed when only ZSM-5 was used. Under this condition, the adsorption capacity of ZSM-5 for Rhodamine B is very low because of the low amount of ZSM-5 (only 0.1 g/L). The photocatalytic activity of only Ag-Fe-ZnO is lower than Ag-Fe-ZnO/ZSM-5. ZSM-5 showed a synergistic positive effect for increasing Rhodamine B degradation. This is because ZSM-5 is advantageous for

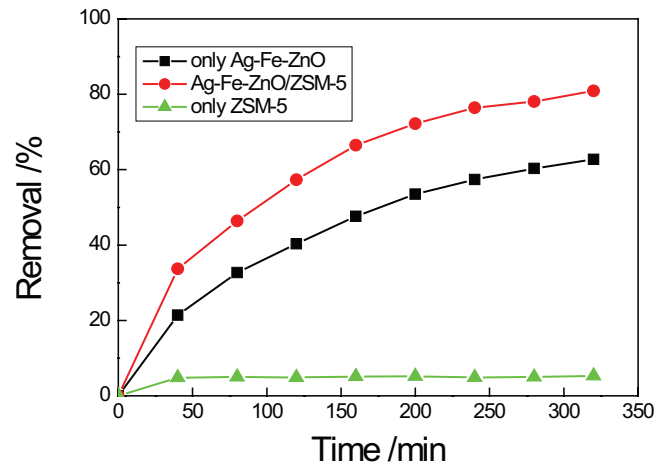


Fig. 7. ZSM-5 impact on Rhodamine B degradation.

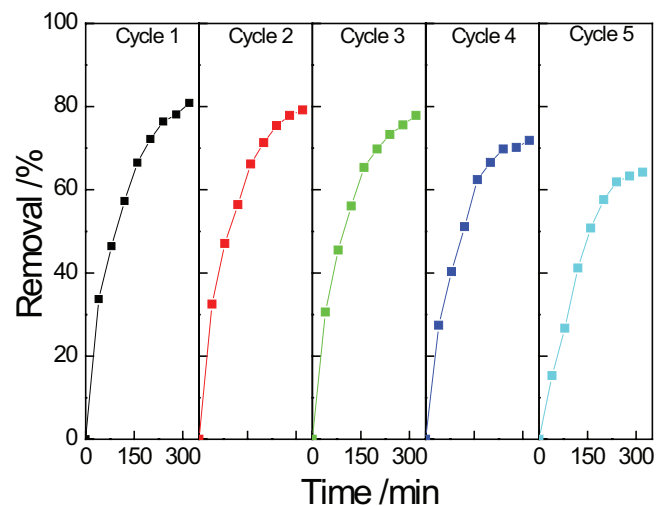


Fig. 8. Recovery test of Ag-Fe-ZnO/ZSM-5 under UV irradiation.

the aggregation of Rhodamine B that occurs from aqueous media to the surface of the catalyst. Only Ag-Fe-ZnO particles without ZSM-5 severely agglomerated, decreasing the catalyst efficiency. ZSM-5 helps to disperse the active ingredient and improves the contact of active site with the contaminants. Therefore, although only ZSM-5 does not show a high adsorption capacity, ZSM-5 combined with Ag-Fe-ZnO shows a synergistic positive effect for the treatment of Rhodamine B.

3.8. Recovery test

Fig. 8 shows the recovery test of Ag-Fe-ZnO/ZSM-5 under UV-light irradiation. The photocatalyst could be used for five times. Almost no decrease in the activity was observed after the first three times. Cycle 5 had a significant decrease with 64% Rhodamine B removal at 320 min. The result shows that Ag-Fe-ZnO/ZSM-5 catalyst is highly stable during the photocatalytic process.

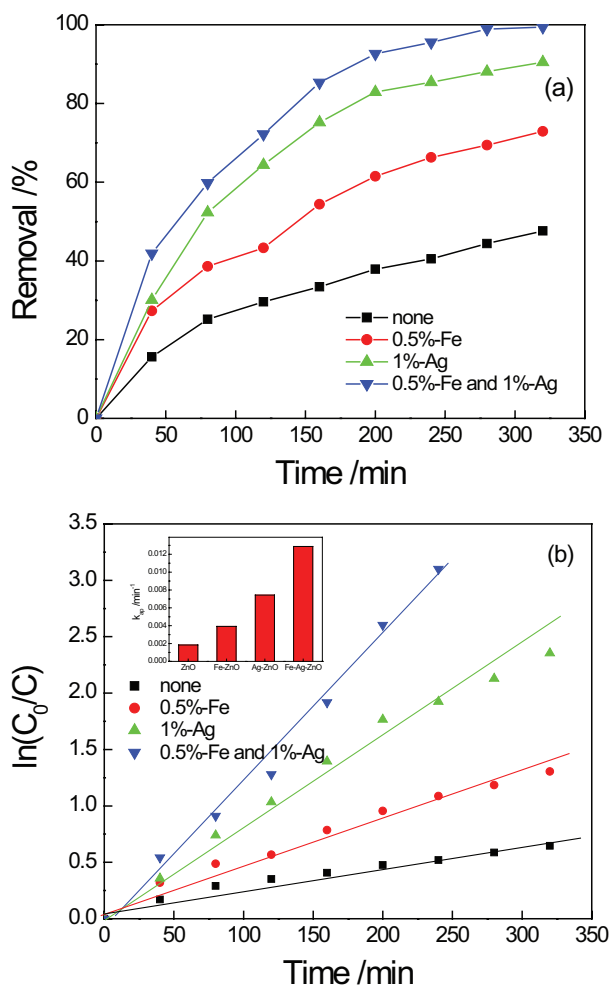


Fig. 9. Reactive Red 6B degradation using different catalysts under UV-light irradiation.

3.9. Degradation of Reactive Red 6B

The chemical structure of Reactive Red 6B containing an azo chemical bond is different from Rhodamine B with a non-azo structure. Fig. 9 shows the photocatalytic activities of ZnO/ZSM-5, Fe–ZnO/ZSM-5, Ag–ZnO/ZSM-5, and Ag–Fe–ZnO/ZSM-5 using Reactive Red 6B as the simulating pollutant under UV-light irradiation. Fig. 9(a) shows that Reactive Red 6B can be completely decomposed using Ag–Fe–ZnO/ZSM-5 catalyst after 280 min. Reactive Red 6B can be easily decomposed than Rhodamine B because an azo band can be easily cleaved than a complex ring structure. Fig. 9(b) shows that the photocatalytic processes also follow first-order kinetics, and the best reaction rate constant is 0.0128 min^{-1} .

4. Conclusions

Four photocatalysts, ZnO/ZSM-5, Fe–ZnO/ZSM-5, Ag–ZnO/ZSM-5, and Ag–Fe–ZnO/ZSM-5 were successfully prepared by the sol–gel method; they exhibited excellent photocatalytic activities in the degradation of Rhodamine B and Reactive Red 6B under UV-light or visible-light irradiation. The ZSM-5 surface showed uniform spherical nano-ZnO

particles with a size of $\sim 10 \text{ nm}$. The BET surface area of Ag–Fe–ZnO/ZSM-5 was $372 \text{ m}^2/\text{g}$. The absorption wavelengths for monometallic-, metallic Fe-, metallic Ag-, and bimetallic Fe- and Ag-loaded ZnO showed a significant redshift phenomenon. The bimetallic Fe- and Ag-loaded ZnO/ZSM-5 had the smallest band-gap energy (3.05 eV) with an incident light wavelength of 407 nm (visible zone). Fe ion and Ag co-loaded nano-ZnO/ZSM-5 effectively suppressed the recombination of photogenerated holes and electrons, thus improving the degradation rate. The best Fe- and Ag-loaded amounts were 0.6% and 1%, respectively, exhibiting 80% Rhodamine B removal at 320 min and 100% Reactive Red 6B removal at 280 min under UV-light irradiation. Ag–Fe–ZnO/ZSM-5 exhibited an outstanding photocatalytic performance under visible-light irradiation with 67% Rhodamine B removal at 320 and 0.0034 min^{-1} reaction rate constant. Ag–Fe–ZnO/ZSM-5 catalyst was highly stable during the photocatalytic process.

Acknowledgments

This work was supported by the National Nature Science Foundation of China (No. 21006057), the Education Technology Equipment and Practice Education in Henan (GZS322), Youth Teacher Support Program of Henan Provincial University (No. 2014GGJS-055), and Henan Provincial Science and Technology Foundation (No. 162300410083).

References

- [1] Y.C. Weng, K.T. Hsiao, Composition optimization of ZnO-based photocatalyst arrays by scanning electrochemical microscopy and characterization of efficient photocatalysts, *Int. J. Hydrogen Energy*, 40 (2015) 3238–3248.
- [2] P. Nakarungsee, G.S. Chen, T.S. Heng, J. Ding, I.M. Tang, S. Talabthong, S. Thongmee, Sb substitution into ZnO nano-composite: ferromagnetic behavior, *J. Magn. Magn. Mater.*, 397 (2016) 79–85.
- [3] A. Behzadnia, M. Montazer, M.M. Rad, In-situ sonosynthesis of nano N-loaded ZnO on wool producing fabric with photo and bio activities, cell viability and enhanced mechanical properties, *J. Photochem. Photobiol., B*, 149 (2015) 103–115.
- [4] Q.L. Wei, H.B. Zhang, Y.Y. Tian, Y.L. Wei, Q. Song, X.Y. Zhou, J. Shao, C.H. Su, Effect of $\text{Er}^{3+}\text{-Yb}^{3+}$ additions on the crystallization and luminescence properties of $\text{ZnO-WO}_3\text{-B}_2\text{O}_3\text{-SiO}_2$ glass ceramics, *J. Alloys Compd.*, 652 (2015) 116–121.
- [5] F.F. Vidor, G.I. Wirth, U. Hilleringmann, Low temperature fabrication of a ZnO nanoparticle thin-film transistor suitable for flexible electronics, *Microelectron. Reliab.*, 54 (2014) 2760–2765.
- [6] S.S. Yi, J.B. Cui, S. Li, L.J. Zhang, D.J. Wang, Y.H. Lin, Enhanced visible-light photocatalytic activity of Fe/ZnO for rhodamine B degradation and its photogenerated charge transfer properties, *Appl. Surf. Sci.*, 319 (2014) 230–236.
- [7] M. Faisal, A.A. Ibrahim, F.A. Harraz, B. Houcine, M.S. Al-Assiri, A.A. Ismail, SnO_2 loaded ZnO nanostructures for highly efficient photocatalyst, *J. Mol. Catal. A: Chem.*, 397 (2015) 19–25.
- [8] H. Xu, T.L. Yu, J.F. Liu, Photo-degradation of Acid Yellow 11 in aqueous on nano-ZnO/Bentonite under ultraviolet and visible light irradiation, *Mater. Lett.*, 117 (2014) 263–265.
- [9] W.G. Xu, S.F. Liu, S.X. Lu, S.Y. Kang, Y. Zhou, H.F. Zhang, Photocatalytic degradation in aqueous solution using quantum-size ZnO particles supported on sepiolite, *J. Colloid Interface Sci.*, 351 (2010) 210–216.
- [10] Y.I. Choi, H.J. Jung, W.G. Shi, Y. Sohn, Band gap-engineered ZnO and Ag/ZnO by ball-milling method and their photocatalytic and Fenton-like photocatalytic activities, *Appl. Surf. Sci.*, 356 (2015) 615–625.

- [11] R. Saleh, N.F. Djaja, UV light photocatalytic degradation of organic dyes with Fe-loaded ZnO nanoparticles, *Superlattices Microstruct.*, 74 (2014) 217–233.
- [12] M. Khatamian, S. Hashemian, A. Yavari, M. Saket, Preparation of metal ion (Fe^{3+} and Ni^{2+}) loaded TiO_2 nanoparticles supported on ZSM-5 zeolite and investigation of its photocatalytic activity, *Mater. Sci. Eng., B*, 177 (2012) 1623–1627.
- [13] W.J. Zhang, L. Du, F.F. Bi, H.B. He, A novel $\text{SrTiO}_3/\text{HZSM-5}$ photocatalyst prepared by sol-gel method, *Mater. Lett.*, 157 (2015) 103–105.
- [14] A.N. Okte, O. Yilmaz, Characteristics of lanthanum loaded TiO_2 -ZSM-5 photocatalysts: decolorization and degradation process of methyl orange, *Appl. Catal., A*, 354 (2009) 132–142.
- [15] Q.Z. Wang, J. Hui, L. Yang, H.H. Huang, Y.X. Cai, S.Q. Yin, Y.M. Ding, Enhanced photocatalytic performance of $\text{Bi}_2\text{O}_3/\text{H-ZSM-5}$ composite for rhodamine B degradation under UV light irradiation, *Appl. Surf. Sci.*, 289 (2014) 224–229.
- [16] P.T. Dou, F.T. Tan, W. Wang, A. Sarreshteh, X.L. Qiao, X.L. Qiu, J.G. Chen, One-step microwave-assisted synthesis of $\text{Ag}/\text{ZnO}/\text{graphene}$ nanocomposites with enhanced photocatalytic activity, *J. Photochem. Photobiol., A*, 302 (2015) 17–22.
- [17] O. Bechambi, M. Chalbi, W. Najjar, S. Sayadi, Photocatalytic activity of ZnO loaded with Ag on the degradation of endocrine disrupting under UV irradiation and the investigation of its antibacterial activity, *Appl. Surf. Sci.*, 347 (2015) 414–420.
- [18] H. Xu, M. Li, J. Zhang, Preparation, characterization, and photocatalytic studies on anatase nano- TiO_2 at internal air lift circulating photocatalytic reactor, *Mater. Res. Bull.*, 48 (2013) 3144–3148.
- [19] H. Xu, F.M. Wu, M. Li, Z.Q. Liang, Application of response surface methodology for optimization of nano- TiO_2 preparation using modified sol-gel method, *J. Sol-Gel Sci. Technol.*, 67 (2013) 394–405.
- [20] C.T. Chang, J.J. Wang, T. Ouyang, Q. Zhang, Y.H. Jing, Photocatalytic degradation of acetaminophen in aqueous solutions by $\text{TiO}_2/\text{ZSM-5}$ zeolite with low energy irradiation, *Mater. Sci. Eng., B*, 196 (2015) 53–60.
- [21] S. Sood, A. Umar, S.K. Mehta, S.K. Kansal, Highly effective Fe-loaded TiO_2 nanoparticles photocatalysts for visible-light driven photocatalytic degradation of toxic organic compounds, *J. Colloid Interface Sci.*, 450 (2015) 213–223.
- [22] J.Z. Ma, H. He, F.D. Liu, Effect of Fe on the photocatalytic removal of NO_x over visible light responsive Fe/TiO_2 catalysts, *Appl. Catal., B*, 179 (2015) 21–28.
- [23] O. Kerkez-Kuyumcu, E. Kibar, K. Dayioglu, F. Gedik, A.N. Akin, S. Ozkara-Aydinoglu, A comparative study for removal of different dyes over M/TiO_2 ($\text{M} = \text{Cu}, \text{Ni}, \text{Co}, \text{Fe}, \text{Mn}$ and Cr) photocatalysts under visible light irradiation, *J. Photochem. Photobiol., A*, 311 (2015) 176–185.